Volume 4, Number 8
1004-423X/95/04080581-14

ACTA PHYSICA SINICA
(Overseas Edition)

August, 1995
©1995 Chin. Phys. Soc.

A CONTINUOUS COMPOUND FOUR-WAVE MIXING MECHANISM FOR SELF-PUMPED PHASE CONJUGATION IN $BaTiO_3$ CRYSTALS*

XIE PING(谢　平), DAI JIAN-HUA(戴建华), WANG PENG-YE(王鹏业),
and ZHANG HONG-JUN(张洪钧)
Institute of Physics, Academia Sinica, Beijing 100080, China

LIN HONG(林　红)
Department of Physics & Astronomy, Bates College, Lewiston, ME 04240, U.S.A.

(Received 25 October 1994)

A continuous compound four-wave mixing mechanism for self-pumped phase conjugation in photorefractive crystals is presented. The coupled-beam equations of this mechanism are solved numerically when depletion of the forward going beam is neglected. The experiment in a Ce-doped $BaTiO_3$ crystal is performed, with the stable phase conjugate reflectivity of as much as $\geq 80\%$. The curved high output phase conjugate intensity are explained using the numerical results.

PACC: 4265F

I. INTRODUCTION

Since the experimental demonstration of self-pumped phase conjugation in a single crystal of $BaTiO_3$ by Feinberg in 1982[1], the attempt to explain its mechanism has been attracted considerable attention in the past years. MacDonald and Feinberg[2] proposed a mechanism that the phase-conjugate wave is generated in two interaction regions by means of a four-wave mixing process with self-generated pump beams. Basing on the work of Zel'dovich et al.[3], Lam[4] suggested a mechanism that the phase-conjugate wave is produced by a process of stimulated backscattering two-wave mixing, and then Valley[5] investigated its phase conjugation fidelity. Chang and Hellwarth[6], and Mullen et al.[7] experimentally demonstrated phase conjugation by this stimulated backscattering using a seed beam scattered either by the side of a cuvette containing the crystal or by a retroreflecting screen which is inserted into the path of the beam after the beam leaves the $BaTiO_3$ crystal. They obtained a stable phase conjugate reflectivity of $\sim 10\%$ and $\sim 60\%$, respectively. Recently, high reflectivities of as much as $70\%-80\%$ have been observed in Ce-doped $BaTiO_3$ crystals, in which there exists no internal reflection at a corner of the crystal as is necessary for the two interaction regions mechanism. All the experiments[6,7] show clearly that the path of

*Project supported by the National Natural Foundation of China, and by the Nonlinear Science Project of China.

the beams follows a curved one. This cannot be explained either by the mechanism of the degenerate four-wave mixing in two coupled interaction regions[2] or by that of stimulated backscattering two-wave mixing.[4] In addition, the stimulated backscattering mechanism cannot explain the high phase conjugate reflectivity as observed by the experiments. Therefore a better explanation of the mechanism responsible for self-pumped phase conjugation is necessary.

In this article, we present a new mechanism to explain self-pumped phase conjugation based on our previous paper.[8] We postulate that the phase conjugate beam at the incident surface of the crystal is produced by a continuous compound four-wave mixing process which can be regarded as an extension of the four-wave mixing process at every point along the beam path inside the crystal. The curved path of the beams and the high intensity of the phase conjugate beam are the direct results of this mechanism.

The proposed mechanism that is responsible for self-pumped phase conjugation and the corresponding coupled-beam equations with boundary conditions describing the evolution of the phase conjugate beam are presented in section II. The experimental results in a Ce-doped $BaTiO_3$ crystal which was grown at the Institute of Physics, Chinese Academy of Sciences, are presented in section III. In section IV, we numerically solve the coupled-beam equations for no depletion of the forward going beam and present some typical results. A discussion of the results and the comparison with backscattering two-wave mixing are also included. Finally, the conclusions are given in section V.

II. THEORY

From our previous paper[8] we know that, when an extraordinary polarized laser beam is input into a photorefractive crystal which has a strong photorefractive effect, it generally follows a curved path. For crystals in which the dominant charge carriers are holes, e.g., $BaTiO_3$ crystal, the beam bends towards the crystal $^+$c-axis. This is caused by the beam coupling between the input beam and the fanning beam in every direction and the coupling between different propagating directions of the fanning beam. (Hereafter we will refer to all the forward propagating beams which include the input beam and its near-forward fanning beam as the forward going beam.) These couplings form a multitude of transmission gratings inside the crystal. When there is a backward going beam which is either seeded by optical inhomogeneities inside the crystal or by an external retroreflector, the backward going beam which also includes many propagating directions will retrace the same path of the forward going beam by the diffraction of those transmission gratings. This is illustrated in fig.1, where fig.1(a) gives the curved path of the forward and backward going beams and fig.1(b) shows the detailed feature of fig.1(a) at a given point inside the crystal. For clarity, in

fig.1(b) we give only two directions of the forward beam 1 and the backward beam 2, their angles with respect to x-axis being α and β.

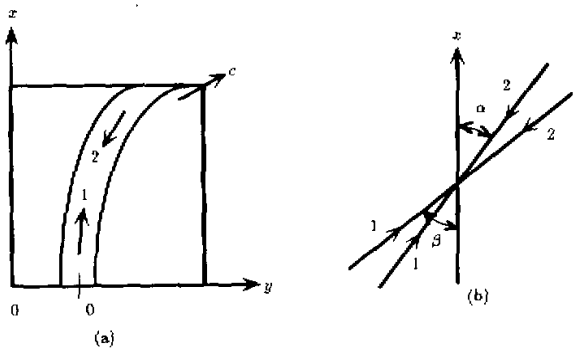

Fig. 1. (a) The curved path of the forward and backward going beams inside a $BaTiO_3$ crystal. (b) Detailed feature of (a) at a given point along the beam path. 1 represents the forward going beam and 2 the backward going beam. Here only two directions are given.

At any point on the whole path for the beams, the different directions of the forward and backward going beams will be coupled with each other through the photorefractive gratings formed by them. These include the transmission gratings formed by different directions of the forward going beam, e.g., $A_1(\alpha)$ and $A_1(\beta)$ or those of the backward going beam, e.g., $A_2(\alpha)$ and $A_2(\beta)$ (where $A_1(\alpha)$ and $A_2(\alpha)$ are the electric field amplitudes of the forward and backward going beams propagating in the α direction, respectively), and the reflection gratings formed by different directions of the forward and backward going beams, e.g., $A_1(\alpha)$ and $A_2(\beta)$, and $A_1(\beta)$ and $A_2(\alpha)$. That is, at every point along the beam path there exists a compound four-wave mixing, which is, in fact, an extension of the four-wave mixing phase conjugation.

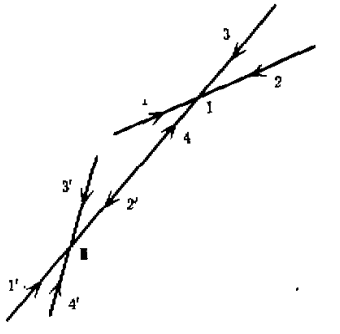

Fig. 2. Diagram to illustrate the continuous evolution of the phase conjugation described in the text.

This compound four-wave mixing occurs continuously as the backward beam travels

along its path. Figure 2 gives a sketch to illustrate this continuous evolution. At point I, the phase conjugate beam 3 of beam 4 is produced with beams 1 and 2 as pump beams, whereas at point II beam 3 (i. e., beam 2′) then serves as a pump beam for phase conjugate beam 3′. By this continuous process the phase conjugate beam of the input beam is finally generated at the incident surface of the crystal.

From the above analysis, with the extension of four-wave mixing[9] to compound four-wave mixing under negligible absorption and following the derivation in Ref.[8], we get the following coupled-beam equations:

$$(\cos\alpha\frac{\partial}{\partial x}+\sin\alpha\frac{\partial}{\partial y})A_1(x,y,\alpha)$$
$$=\int_0^{\frac{\pi}{2}}\{\frac{\gamma_1(\alpha,\beta)}{I_0}[A_1(x,y,\alpha)A_1^*(x,y,\beta)+A_2^*(x,y,\alpha)A_2(x,y,\beta)]A_1(x,y,\beta)$$
$$+\frac{\gamma_2(\alpha,\beta)}{I_0}[A_1(x,y,\alpha)A_2^*(x,y,\beta)+A_2^*(x,y,\alpha)A_1(x,y,\beta)]A_2(x,y,\beta)\}\mathrm{d}\beta\ , \qquad (1a)$$
$$(\cos\alpha\frac{\partial}{\partial x}+\sin\alpha\frac{\partial}{\partial y})A_2^*(x,y,\alpha)$$
$$=\int_0^{\frac{\pi}{2}}\{\frac{\gamma_1(\alpha,\beta)}{I_0}[A_1(x,y,\alpha)A_1^*(x,y,\beta)+A_2^*(x,y,\alpha)A_2(x,y,\beta)]A_2^*(x,y,\beta)$$
$$+\frac{\gamma_2(\alpha,\beta)}{I_0}[A_1(x,y,\alpha)A_2^*(x,y,\beta)+A_2^*(x,y,\alpha)A_1(x,y,\beta)]A_1(x,y,\beta)\}\mathrm{d}\beta\ , \qquad (1b)$$
$$I_0=\int_0^{\frac{\pi}{2}}[|A_1(x,y,\alpha)|^2+|A_2(x,y,\alpha)|^2]\mathrm{d}\alpha\ , \qquad (1c)$$

where $|A_1(x,y,\alpha)|^2$ and $|A_2(x,y,\alpha)|^2$ are the intensity distributions per radian of the forward and backward going beams, respectively, in the α direction at position (x,y) as defined in Ref.[8]. $A_1(x,y,\alpha)$ and $A_2(x,y,\alpha)$ are correspondingly the electric field amplitudes of the forward and backward going beams propagating in the α direction at (x,y). The first term in the integral on the right-hand side of Eq.(1a) or (1b) describes the effect of the transmission gratings, and the second one describes the effect of the reflection gratings. I_0 is the total light intensity inside the crystal, $\gamma_1(\alpha,\beta)$ is the beam-coupling coefficient between $A_1(x,y,\alpha)$ and $A_1(x,y,\beta)$, or between $A_2(x,y,\alpha)$ and $A_2(x,y,\beta)$, while $\gamma_2(\alpha,\beta)$ is the beam-coupling coefficient between $A_1(x,y,\alpha)$ and $A_2(x,y,\beta)$, or between $A_1(x,y,\beta)$ and $A_2(x,y,\alpha)$.

The boundary conditions are as follows:

$$A_1(0,y,0)=A_1^{(0)}\exp(-\frac{y^2}{2d^2})\ , \qquad \alpha=0 \qquad (2a)$$
$$|A_1(0,y,\alpha)|=\sqrt{\varepsilon_1}|A_1(0,y,0)|\ , \qquad \alpha\neq=0 \qquad (2b)$$

$$|A_2(L,y,\alpha)| = \sqrt{\varepsilon_2}|A_1(L,y,\alpha)| \ . \tag{2c}$$

Equation (2a) shows that the input beam has a Gaussian profile, with a waist d (defined as the width at which the input field declines to $1/e$ of its peak value); ε_1 is the scattering coefficient describing the fanning of input beam $A_1(0,y,0)$ into the scattered fanning beam at the incident surface $x = 0$; ε_2 is the retroreflecting (or scattering) coefficient of the forward going beam at the exit surface $x = L$. The random phases of different propagating directions of the scattered beams are not considered, for the phases of the interacting beams do not affect their intensities in photorefractive four-wave mixing[10] and we only consider intensities here.

The coupling coefficient $\gamma_i(\alpha,\beta)(i = 1,2)$ is given by[11]

$$\gamma_i(\alpha,\beta) = \frac{\omega}{2n_e c} r_{i\text{eff}}(\alpha,\beta) E_{isc}(\alpha,\beta) \ , \tag{3}$$

where for extraordinary polarization the effective electrooptic coefficient $r_{i\text{eff}}(\alpha,\beta)$ is[12]

$$\begin{aligned} r_{i\text{eff}}(\alpha,\beta) = &\frac{1}{2}\{n_o^4 r_{13}[\cos 2\theta_i - \cos 2\theta_{ic}] + 4n_e^2 n_o^2 r_{42}\sin^2\theta_{ic} \\ &n_e^4 r_{33}[\cos 2\theta_i + \cos 2\theta_{ic}]\}\cos\theta_{ic} \ . \end{aligned} \tag{4}$$

here ω is the optical frequency, c is the speed of light, $r_{jk}(j,k = 1,2,3)$ are the electrooptic coefficients, and n_o and n_e are the ordinary and extraordinary refractive indices; θ_i are the half angles between the two coupling beams, and θ_{ic} are the angles between the c-axis and the grating wave vectors K_i, which means $K_1 = k_1(\beta) - k_1(\alpha) = k_2(\alpha) - k_2(\beta)$ or $K_2 = k_1(\alpha) - k_2(\beta) = k_1(\beta) - k_2(\alpha)$. In the absence of applied or intrinsic electric fields, the space charge electric field is given by

$$E_{isc}(\alpha,\beta) = \frac{k_B T}{q}\frac{K_i}{1 + K_i^2/K_{i0}^2}\xi_i \ , \tag{5}$$

where $k_B T$ is the thermal energy and q the charge of the mobile charge carriers. $\xi_1 = e_\alpha \cdot e_\beta$ and $\xi_2 = -e_\alpha \cdot e_\beta$, with e_α and e_β being the unit polarization vectors of the forward going beam in the α and β directions, respectively. K_{i0} is a constant of the material that depends on the number density N of available charge carriers

$$K_{i0} = \left(\frac{N_q^2}{\varepsilon_i \varepsilon_0 k_B T}\right)^{\frac{1}{2}} \ , \tag{6}$$

where ε_0 is the permittivity of free space and ε_i is the relative dielectric constant at low frequency ($\leq$1Hz) along the direction of the grating wave vector K_i, with its value equal to

$$\varepsilon_i = \varepsilon_c \cos^2\theta_{ic} + \varepsilon_a \sin^2\theta_{ic} \ . \tag{7}$$

Here ε_c and ε_a are relative dielectric constants parallel and perpendicular to the crystal c-axis, respectively.

III. EXPERIMENT

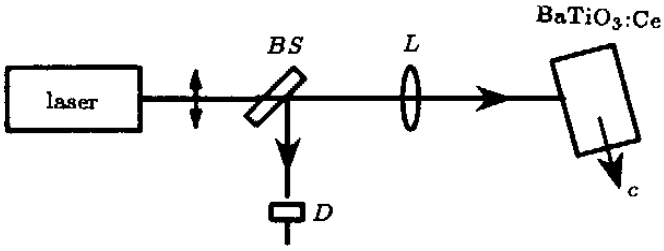

Fig. 3. Experimental setup used for measuring the phase conjugate reflectivity in a Ce doped $BaTiO_3$ crystal. *BS*: beamsplitter; *L*: focusing lens.

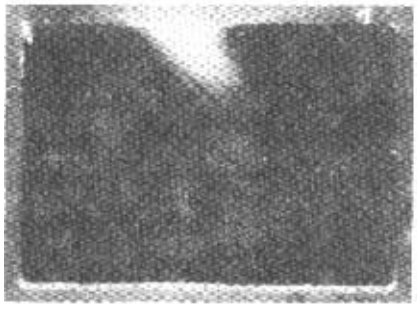

Fig. 4. Photograph of the beam path inside a $BaTiO_3$:Ce crystal after the buildup of the steady-state for a wavelength of 514.5 nm.

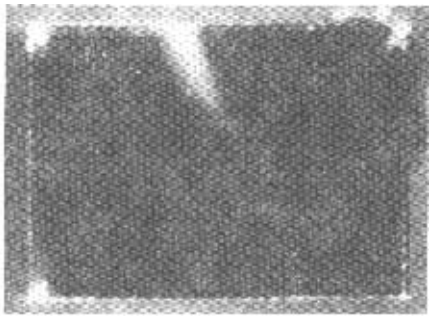

Fig. 5. Photograph of the beam path inside a $BaTiO_3$:Ce crystal after the buildup of the steady-state for a wavelength of 632.8 nm.

The crystal used in the experiment was a Ce-doped $BaTiO_3$ (30 ppm), which was grown at the Institute of Physics, Chinese Academy of Sciences. Its dimensions were 7.39 mm×5.20mm ×5.21 mm, with its *c*-axis along the 7.39 mm edge. We used two wavelengths of 514.5 and 632.8 nm in the experiment. The experimental setup is shown in Fig.3. An extraordinary beam from an Ar^+ laser or a He-Ne laser passes through a beam splitter *BS* and a focusing lens *L*, and is then incident upon the $BaTiO_3$:Ce crystal at an angle of 68° with respect to the normal to the crystal surface. The power of the incident beam is 10 mW at 514.5 nm and 2.6 mW at 632.8 nm, and the beam diameter is about 1 mm as it enters the crystal. The intensity of the phase conjugate beam, after reflection from the beam splitter *BS*, is measured by a detector *D*. For the wavelength of 514.5 nm, the stable phase conjugate beam was obtained after about 4 minutes, with a reflectivity of $\sim$ 70% (The Fresnel losses were not considered). Figure 4 is the photograph of the beam path inside the $BaTiO_3$:Ce crystal after the buildup of its steady-state. For the wavelength of 632.8 nm, a stable phase conjugate reflectivity of $\leq$ 80% was obtained after about 20 minutes. Figure 5 is a photograph of its path. It is seen that the path of the forward and backward going beams is curved. This cannot be explained by the stimulated backscattering two-wave mixing mechanism. It also clearly shows that there is no internal reflection at a corner of the crystal as is in the case

of the two coupled interaction regions mechanism. Therefore we suggest a new mechanism which will be described in the next section.

IV. RESULTS AND DISCUSSION

Equations (1) are too complicated to be solved analytically and thus difficult to be solved numerically. The problem may be simplified by making an assumption that forward going beam is undepleted. That is, in the calculation of the propagation of the forward going beam, the effect of the backward going beam is negligible. And Eq.(1a) is then simplified to

$$(\cos\alpha\frac{\partial}{\partial x}+\sin\alpha\frac{\partial}{\partial y})A_1(x,y,\alpha)$$

$$=\int_0^{\frac{\pi}{2}}\frac{\gamma_1(\alpha,\beta)}{I_0}A_1(x,y,\alpha)A_1^*(x,y,\beta)A_1(x,y,\beta)\mathrm{d}\beta\,, \tag{7a}$$

$$I_0=\int_0^{\frac{\pi}{2}}|A_1(x,y,\alpha)|^2\mathrm{d}\alpha\,, \tag{7b}$$

which is similar to the case in Ref.[8].

For a $BaTiO_3$ crystal at an input wave length λ of 514.5 nm, one has $n_o = 2.488$ and $n_e = 2.424$. The charge is $q = +1.6\times10^{-19}$C. The nonzero, linear electro-optic coefficients are $r_{13} = 33$, $r_{33} = 124$ and $r_{42} = 1640$, in units of pm/V. The relative dielectric constants parallel and perpendicular to the c-axis are $\varepsilon_c = 135$ and $\varepsilon_a = 3600$, respectively. The available charge carrier number density is $N = 8\times10^{22}\,\mathrm{m}^{-3}$[13,14]. For a $BaTiO_3$:Ce crystal, we do not know its definite optical parameters up to now. Since the doping concentration of cerium is very small (30 ppm), it almost has no influence on the parameters of the ordinary and extraordinary refractive indices, electro-optic coefficients and the dielectric constants; only the charge carrier number density is slightly increased. So we assume here the parameters for $BaTiO_3$:Ce are identical to those for an undoped $BaTiO_3$ except that the charge carrier number density N is larger (estimated by the two-beam-coupling coefficient measurement in $BaTiO_3$:Ce).

The above equations were solved numerically by the finite-difference method used in Ref.[8], with 500 grid points. In the calculation of Eq.(1b) the values of $A_1(x,y,\alpha)$ were taken as those calculated in Eq.(7).

Throughout the calculation the crystal thickness was set to $L = 5$ mm; the fanning scattering coefficient ε_1 was assumed to be 10^{-6}, the maximum of the input Gaussian beam $A_1^{(0)} = 100$ in arbitrary units, and the beam waist $d = 1$ mm.

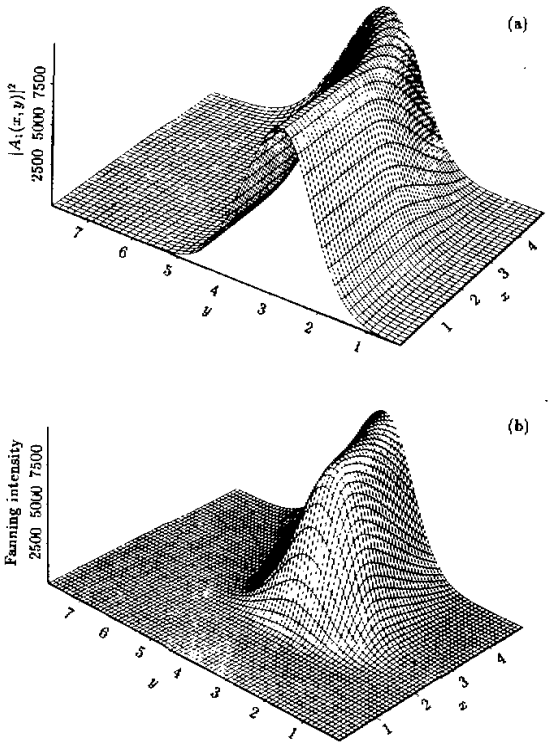

Fig. 6. The intensity distribution of (a) the forward going beam and (b) the fanning beam inside an undoped $BaTiO_3$ crystal for a 45°-orientation. The origin of the y axis is shifted 3 mm relative to that given in Eq.(2a).

Figure 6(a) shows the intensity distribution of the forward going beam inside an undoped $BaTiO_3$ crystal ($I_1(x,y) = \int_0^{\pi/2} |A_1(x,y,\alpha)|^2 \mathrm{d}\alpha$) for a 45°-orientation (the internal angle between the crystal c-axis and the direction of the input beam being 45°). The vertical axis represents the light intensity and the other two axes are x and y in mm. It is seen that the beam goes along a curved path as observed in the experiment. In Fig.6(b) we give only the intensity distribution of the fanning beam[8] inside the crystal. We see that the fanning beam begins to increase rapidly at $x = 1.8$ mm and attains its maximum value at $x = 2.8$ mm. After that it bends towards the crystal c-axis. Figure 7(a) is the graph of the intensity distribution of the backward going beam inside the crystal. Considering that there exists extra seeding by the a side of a cuvette in Ref.[6] and by a retroreflecting screen in Ref.[7], we assume here the coefficient ε_2 is a little larger than ε_1, i.e., $\varepsilon_2 = 10^{-4}$.

From the figure we observe that at $x > 3.4\,\text{mm}$ the backward going beam intensity is very small. Between $x = 3.4 - 1.8\,\text{mm}$ it increases very rapidly. The important feature to be noted here is that the region in which the backward going beam rapidly increases (or is rapidly amplified) is behind that in which the near forward going beam rapidly increases (or is rapidly amplified) is behind that in which the near forward fanning beam of the input beam begins to rapidly increase (or be rapidly amplified). From Fig.7(a) we also note that the backward going beam follows a curved path, which is in accordance with that observed

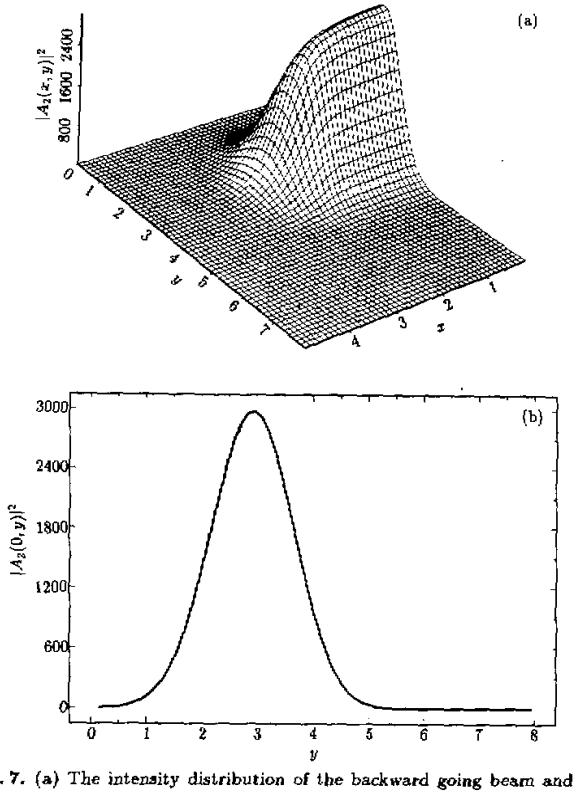

Fig. 7. (a) The intensity distribution of the backward going beam and (b) the output phase conjugate intensity as a function of y at the incident surface $x = 0$ for the case in Fig.6.

in experiments. In Fig.7(b) we plot the intensity of the output backward beam (the phase-conjugate beam of the input beam) at $x = 0$, i.e., $|A_2(0, y, 0)|^2$ as a function of y. The numerical results show that the intensity of the backward beam in other directions $\alpha \neq 0$ at $x = 0$ are small. It is seen from Fig.7(b) that the intensity of the output phase-conjugate beam is 30% of the input intensity. It should be pointed out that the larger the coefficient

ε_2, the larger the output phase-conjugate intensity, which is resulted from the undepleted approximation of the forward going beam.

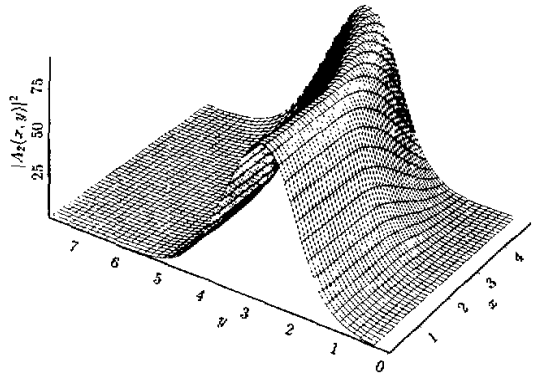

Fig. 8. The intensity distribution of the backward going beam *when only transmission gratings are operative for the case in Fig.6.*

When only transmission gratings are operative, the backward going beam will not be amplified and it only retraces the same curved path of the forward going beam due to the diffraction effect of the transmission gratings. This assertion is verified by the numerical results of Eq.(1), as shown in Fig.8, which gives the intensity distribution of the backward going beam at all points (x, y) inside the crystal (with ε_2 assumed to be 10^{-2} now). From the figure it can be clearly seen that the path of the backward going beam exactly coincides with that of the forward going beam. We can thus conclude that the amplified output phase-conjugate intensity is the result of the simultaneous operation of both the transmission and the reflection gratings.

The results presented above are for the undoped $BaTiO_3$ crystal. In the following we will give some typical results and discussion for a Ce-doped $BaTiO_3$ crystal. In Fig.9(a) we show the intensity distribution of the forward going beam in a $BaTiO_3$:Ce crystal of available charge carrier number density $N = 1.6 \times 10^{23}\,\mathrm{m}^{-3}$ for a 35°-orientation and in Fig.9(b) we show that of the backward going beam. Figure 9(c) is the output phase-conjugate intensity at $x = 0$. Considering that in the experiments in Ce-doped $BaTiO_3$ crystals there is no extra seeding by external retroreflectors, we assume the coefficient ε_2 to be much smaller than that given in undoped $BaTiO_3$ crystals, i.e., $\varepsilon_2 = 10^{-8}$ here after. Figures 10(a) and 10(b) show the intensity distributions of the forward going beam and backward going beam, respectively, in a $BaTiO_3$:Ce of $N = 2 \times 10^{23}\,\mathrm{m}^{-3}$ for a 35°-orientation. In Fig.10(c) we give the output phase-conjugate intensity increases greatly with the increase of the available charge carrier number density. The much higher output intensity of more than 4 times that of the input intensity s due to the fact that in the calculation of $|A_2(x, y, \alpha)|^2$ the

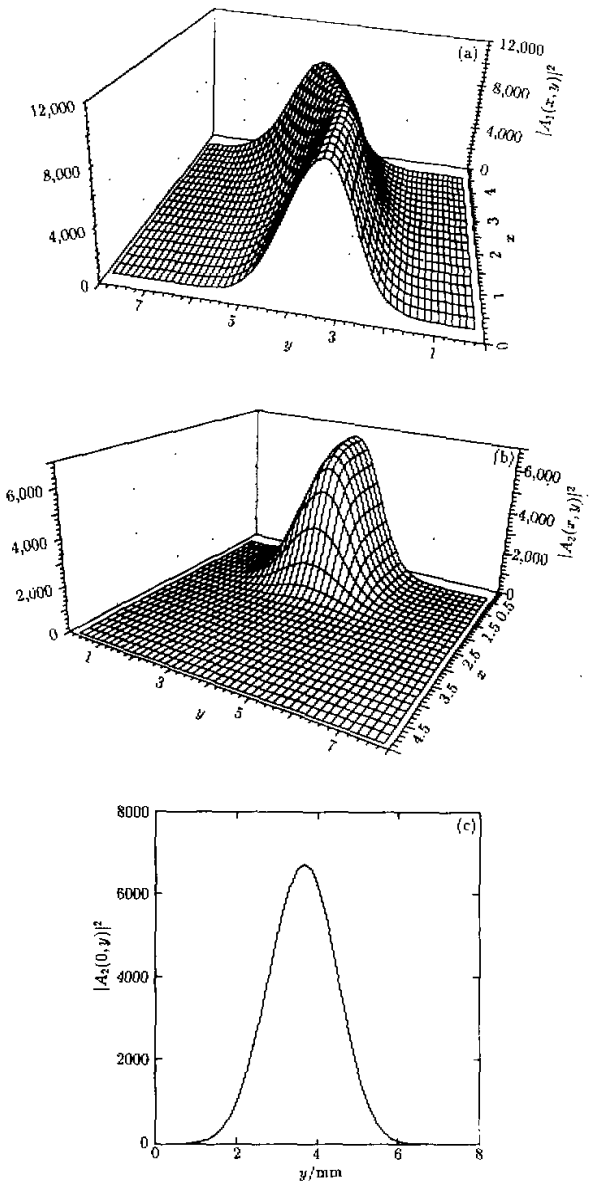

Fig. 9. The intensity distribution of the (a) forward and (b) backward going beams inside a $BaTiO_3$:Ce of available charge carrier number density $1.6 \times 10^{23}\,m^{-3}$ for a 35° -orientation; (c) the output phase conjugate intensity as a function of y at $x = 0$. The origin of the y axis is shifted 3.5 mm relative to that given in Eq.(2a).

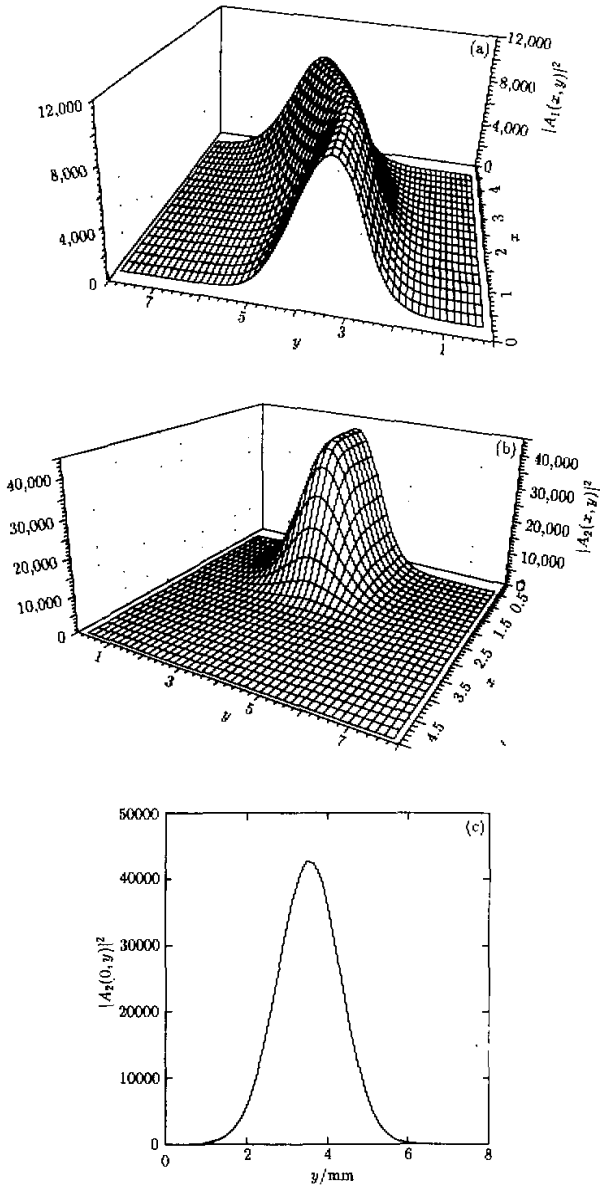

Fig. 10. The intensity distribution of the (a) forward and (b) backward going beams inside a $BaTiO_3$:Ce of available charge carrier number density $2 \times 10^{23}\,m^{-3}$ for a 35°-orientation; (c) the output phase conjugate intensity as a function of y at $x = 0$. The shift of the y axis origin is the same as that in Fig.9.

forward going beam amplitudes are assumed to be undepleted. The curved paths of the forward and backward going beams shown in the figures are in accordance with the experiments, as shown in Figs.4 and 5. The high phase-conjugate reflectivities of as much as $\geq 80\%$, as described in section Ⅲ, are understandable by the very high value of the calculated output phase-conjugate intensities, as shown in Figs9(c) and 10(c).

To compare with the backscattering two-beam coupling mechanism, we will discuss the effect of 2-K grating as follows.

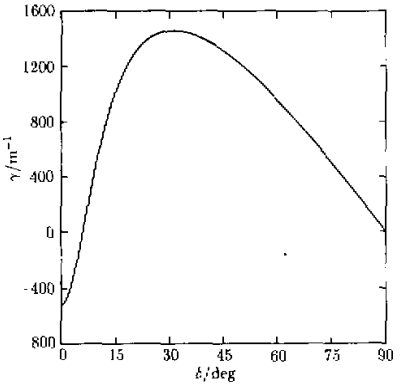

Fig. 11. Two-beam coupling coefficient of two counterpropagating beams versus the internal incident angle δ.

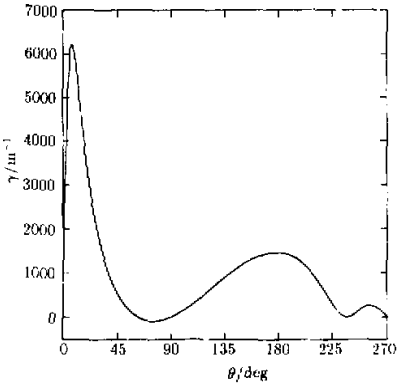

Fig. 12. Two-beam coupling coefficient versus the internal angle θ between the input beam and the scattered beam.

Using Eqs.(3)-(6) and the parameters for an undoped $BaTiO_3$ crystal given above, we plot in Fig.11 the two-beam coupling coefficient of two counterpropagating beams as a function of the incident angle δ, which is defined as the internal angle between the crystal c-axis and the direction of the input beam. It is seen that the maximum coupling coefficient occurs at $\delta = 31°$. For this incident angle ($\delta = 31°$) we plot in Fig.12 the two-beam coupling coefficient as a function of the internal angle θ between the input beam and the scattered beam. We see that the coupling coefficient for the two forward beams is much larger than that for the two counterpropagating beams, which means that forward beam fanning is much stronger than that for the backward. Therefore, the backward phase-conjugate beam cannot obtain a high gain from the input beam. Even if the forward and other directions (the near backward) of the beam fanning are not considered, the backward beam will be 0.1466 times that of the input beam for $\varepsilon_2 = 10^{-4}$ with no depletion of the input beam and the interaction length of 5 mm. This is smaller than that given in Fig.7(b). For a $BaTiO_3$ of $N = 1.6 \times 10^{23}\,m^{-3}$, the backward beam intensity will be 1.73×10^{-2} times that of the input beam intensity at the incident surface for $\varepsilon_2 = 10^{-8}$. This is much smaller than that

calculated by the above mechanism [compare with Fig.9(c)].

V. CONCLUSION

In summary, we have proposed a continuous compound four-wave mixing mechanism to explain the self-pumped phase conjugation in photorefractive crystals and have numerically solved its coupled-beam equations for no depletion of the forward going beam. The experimental studies of this phase conjugation were performed at wavelengths of 514.5 and 632.8 nm in a Ce-doped $BaTiO_3$ crystal with doping concentration 30 ppm. Stable reflectivities of $\geq 80\%$ have been observed. The theoretical results show that the forward and backward going beams follow a curved path as demonstrated in the experiments. The numerical results revealed that the region in which the backward going beam increases rapidly is behind that in which the near forward fanning beam of the input beam begins to rapidly increase. The numerical results show that the output phase conjugate intensity increases greatly with increase of the available charge carrier number intensity. This explains the high phase conjugate reflectivities measured in Ce doped $BaTiO_3$ crystals. A solution of the coupled-beam equations of this mechanism taking into account depletion of the forward going beam will be further studied.

ACKNOWLEDGMENTS

Dai Jian-hua gratefully acknowledges the support of K. C. Wang Education Foundation, Hong Kong and Lin Hong gratefully acknowledges the support of the Research Corporation, U. S. A.

REFERENCES

[1] J. Feinberg, *Opt. Lett.*, **7**(1982), 486.
[2] K. R. MacDonald and J. Feinberg, *J. Opt. Soc. Am.*, **73**(1983), 548.
[3] B. Ya. Zel'dovich, N. F. Pilipetsky and V. V. Shkunov, Principles of Phase Conjugation (Springer-Verlag, New York, 1985).
[4] J. F. Lam, *Appl. Phys. Lett.*, **46**(1985), 909.
[5] G. C. Valley, *J. Opt. Soc. Am.*, **B9**(1992), 1440.
[6] T. Y. Chang and R. W. Hellwarth, *Opt. Lett.*, **10**(1985), 408.
[7] R. A. Mullen, D. J. Vickers, L. West and D. M. Pepper, *J. Opt. Soc. Am.*, **B9**(1992), 1726.
[8] P. Xie, J. H. Dai, P. Y. Wang and H. J. Zhang, *J. Appl. Phys.*, **75**(1994), 1891.
[9] B. Fischer, M. Cronin-Golomb, J. O. White and A. Yariv, *Opt. Lett.*, **6**(1981), 519; M. Cronin-Golomb, B. Fischer, J. O. White and A. Yariv, *IEEE J. Quantum Electron.*, **QE-20**(1984), 12.
[10] P. Xie, J. H. Dai and H. J. Zhang, *J. Opt. Soc. Am.*, **B9**(1992), 2240.
[11] N. K. Kukhtarev, V. B. Markov, S. G. Odulov, M. S. Soskin and V. L. Vinetskii, *Ferroelectrics*, **22**(1979), 949.
[12] Y. Fainman, E. Klancnik and S. H. Lee, *Opt. Eng.*, **25**(1986), 228.
[13] S. Ducharme and J. Feinberg, Electrooptic and Piezoelectric Measurements in Photorefractive Materials, 1986 Annual Meeting, Optical Society of America, p. 25.
[14] P. Yeh, Introduction to Photorefractive Nonlinear Optics (John Wiley & Sons, Inc., New York 1993).